Contents list available at CBIORE journal website

International Journal of Renewable Energy Development

Journal homepage: https://ijred.cbiore.id

Research Article

Structural, morphological and optical properties of ZnO thin films grown by time-dependent chemical bath deposition

Alphonse Déssoudji Gboglo[a,b], Mazabalo Baneto[a,b*], Ognanmi Ako[a,b], Komlan Segbéya Gadedjisso-Tossou[a,c], Bruno Grandidier[d], Muthiah Haris[e], Muthuswamy Senthilkumar[e], Kekeli N'Konou[d*]

[a] *Centre d'Excellence Régional pour la Maîtrise de l'Electricité (CERME), University of Lomé, 01BP 1515, Lomé, Togo*

[b] *Laboratory on Solar Energy, Department of Physics, Faculty of Sciences, University of Lomé, 01BP 1515, Lomé, Togo*

[c] *Physics of Semiconductor Materials and Components Laboratory, Department of Physics, Faculty of Sciences, University of Lomé, 01BP 1515, Lomé, Togo*

[d] *University of Lille, CNRS, Centrale Lille, Polytechnique Hauts-de-France, Junia-ISEN, UMR 8520 - IEMN, F-59000 Lille, France*

[e] *School of Arts and Natural Sciences, Joy University, Raja Nagar, Vadakangulam, Near Kanyakumari, Tirunelveli Dist.-627116, Tamil Nadu, India*

Abstract. This study investigates the effect of deposition time on the structural, morphological, and optical properties of ZnO thin films synthesized by single-step chemical bath deposition (CBD) without the use of a seed layer. The films were systematically characterized using X-ray diffraction (XRD), scanning electron microscopy (SEM), Fourier-transform infrared spectroscopy (FTIR), and UV-Visible spectroscopy in order to establish correlations between growth conditions and film properties. XRD analysis confirmed that all synthesized films are polycrystalline and crystallize in the hexagonal wurtzite structure, with average lattice parameters of a = 3.247 Å and c = 5.209 Å. The crystallite size increased slightly from 13.27 nm to 14.05 nm with increasing deposition time, indicating improved structural ordering and crystallinity. FTIR spectra verified the presence of characteristic Zn–O vibrational modes together with surface hydroxyl groups and other functional bonds related to the growth process. SEM images revealed a strong dependence of surface morphology on deposition time: ZnO microrods evolved from loosely distributed to more compact and densely packed assemblies as the deposition progressed, confirming enhanced film coverage. Optical measurements highlighted significant modifications in the transparency and band structure of the films. The average optical transmittance in the visible range decreased progressively from 68% to 52% when deposition time was extended from 30 to 120 minutes, reflecting increased film density. Concurrently, the optical band gap narrowed from 3.27 eV to 3.22 eV. These findings demonstrate that single-step CBD provides a reliable and controllable route for synthesizing ZnO thin films with tunable physical properties.

Keywords: thin film; zinc oxide; mesoporous; physical properties; deposition time; single-step chemical bath deposition

Received: 12th August 2025; Revised: 18th Oct 2025; Accepted: 16th Nov 2025; Available online: 5th Dec 2025

1. Introduction

In recent years, transparent conductive oxides (TCOs) have gained significant attention in the fields of electronics and optics due to their excellent visible light transparency and high electrical conductivity (Hosono *et al.*, 2017). These exceptional characteristics make TCOs essential for a wide range of technological applications, including solar cells (Hamelmann, 2014), light-emitting diodes (Liu *et al.,* 2010), photoelectrocatalysts (Wen *et al.,* 2024) and optical sensors (Ohodnicki *et al.*, 2013). Among the various TCO materials, zinc oxide (ZnO) stands out as a promising candidate for next-generation photovoltaic technologies, particularly in dye-sensitized solar cells (DSSCs), where it serves as an effective photoanode material. Although titanium dioxide (TiO_2) remains the most commonly used material in this field, ZnO has emerged as a promising alternative due to its similar wide band gap (3.37 eV for ZnO vs. 3.2 eV for TiO_2) (Parihar *et al.*, 2018; Wu *et al.*, 2018), comparable conduction band edge (Gan *et al.,* 2020; He *et al.*, 2015), and advantageous electronic properties such as high exciton binding energy (60 meV) (Hassan *et al.,* 2014), greater electron mobility (205 $cm^2.V^{-1}.s^{-1}$) (Look *et al.,* 1998), and longer electron lifetime (Aksoy *et al.*, 2020). These features make ZnO particularly attractive for enhancing charge collection and improving light harvesting in DSSCs. Among the different morphologies of ZnO, mesoporous thin films have attracted considerable attention due to their high surface area, which favors dye adsorption and electron transport in DSSCs (Kim *et al.*, 2016; Kuo *et al.,* 2014).

The deposition methods used to synthesize ZnO thin films play a crucial role in determining their final properties, thus influencing the overall efficiency of DSSCs. A wide range of deposition methods has been utilized for ZnO thin film fabrication, such as magnetron sputtering (Lupan *et al.,* 2012), physical vapor deposition (George *et al.*, 2010), chemical vapor deposition (Schaper *et al.*, 2021), sol-gel processing (Xiao-bo *et al.,* 2007), sonochemical synthesis (Khorsand Zak *et al.,* 2013),

* Corresponding authors
Email: mazbaneto@gmail.com (M. Baneto); kekeli.nkonou@junia.com (K. N'konou)

https://doi.org/10.61435/ijred.2026.61665
ISSN: 2252-4940/© 2026.The Author(s). Published by CBIORE

doctor blade coating (Magiswaran *et al.,* 2022), electrodeposition (Xu *et al.,* 2023), spray pyrolysis (Ako et al., 2025), hydrothermal synthesis (Elen *et al.*, 2009) and chemical bath deposition (CBD) (Gboglo, Baneto, Gadedjisso-Tossou, *et al.,* 2025). Among these, CBD stands out as a low-cost and low-temperature approach that can be performed under atmospheric conditions. It is especially suitable for producing ZnO nanostructures directly on substrates such as glass. Additionally, CBD provides flexibility in controlling film characteristics by adjusting parameters like precursor concentration, pH, bath temperature, and deposition time (Fekadu *et al.*, 2019; Gboglo, Baneto, Ako, *et al.,* 2025).

Despite its advantages, the CBD presents challenges in precisely controlling the size, morphology, and orientation of ZnO nanostructures, especially nanorods (Wang *et al.,* 2009). To address this, a two-step method is often employed, involving the deposition of a ZnO seed layer (via spin coating or spray pyrolysis), followed by the CBD growth step (N Rosli *et al.,* 2020; Tirtha *et al.*, 2022). Several studies have examined how deposition time during the CBD growth step (second step process) affects the resulting ZnO properties. For example, Liyana *et al.* (Liyana *et al.*, 2020) observed that increasing the growth time of a few hours reduced both the electrical resistivity and optical transmittance of ZnO nanorods, indicating a trade-off between conductivity and transparency. Rahman *et al.* (Rahman *et al.,* 2019) reported a decrease in transmittance as deposition time increased from 1 to 3.5 hours for flower-shaped ZnO nanorods. Similarly, Ungula *et al.* (Ungula *et al.*, 2024) found that 90 minutes was the optimal growth time for obtaining ZnO nanorods suitable for DSSC photoanodes on Ga-doped ZnO substrates, but their films still exhibited transmittance below 50% due to the two-step method used. These findings highlight the persistent challenge of achieving both mesoporous structure and high transparency in ZnO films for photovoltaic applications.

Although mesoporous ZnO thin films have been studied in previous works, most of their synthesis has predominantly been performed in basic reaction environments (pH 8-11) (Arellano-Cortaza *et al.,* 2021; Gboglo, Baneto, Gadedjisso-Tossou, *et al.,* 2025). In this context, it seems appropriate to revisit the growth strategy by exploring a single-step CBD, focusing on optimizing the deposition time, a fundamental parameter for achieving a compromise between porosity, crystallinity and transparency. This approach aims to synthesize uniform, well crystallized and highly transparent ZnO thin films without a seed layer, thereby simplifying the synthesis process. This study explores how deposition time affects the morphological, structural, and optical properties of ZnO thin films synthesized through a single-step CBD process.

2. Experimental details

2.1 Materials and reagents

Glass substrates were used to synthesize various ZnO thin films. All chemical materials employed, such as Zinc Nitrate Hexahydrate[$Zn(N_2O_6).6H_2O$] and Hexamethylenetetramine (HMTA) [$(CH_2)_6N_4$] were purchased at ISOCHEM, while Sodium hydroxide pellets were provided by Sigma-Aldrich (Merck Group). Ethanol (C_2H_6O), acetone[$(CH_3)_2CO$] and distilled water were used as solvents. All chemicals were of analytical reagent (AR) grade with a purity greater than 99% and were used without any additional purification.

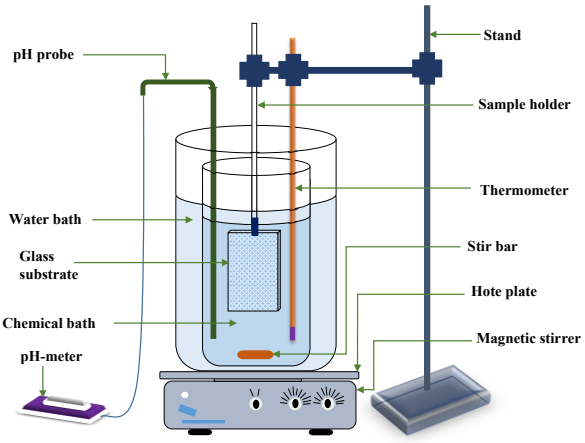

Fig. 1 Chemical bath deposition device.

2.2 Synthesis of ZnO thin films

A single-step CBD technique (Fig.1) was utilized to synthesize ZnO thin films. The precursor solution consisted of an equimolar mixture of an aqueous solution of HMTA and [$Zn(N_2O_6).6H_2O$]. Glass substrates were cleaned sequentially in an ultrasonic bath using acetone, ethanol, and distilled water for 15 minutes each. Following the cleaning process, the substrates were dried under a stream of nitrogen gas (N_2). Both [$Zn(N_2O_6).6H_2O$] and HMTA used as precursors, were dissolved individually in the distilled water at a concentration of 0.3M. Fig. 2 outlines the complete process of ZnO thin films synthesis. The prepared aqueous solutions were mixed using a magnetic stirrer to ensure a homogeneous and transparent solution. Sodium hydroxide was gradually added to adjust the pH to 8, resulting in the formation of a milky-white mixture. Stirring was continued on a hot plate with magnetic agitation. The cleaned glass substrates were vertically immersed in the precursor solution, ensuring no contact with the beaker walls. ZnO thin films were synthesized at a temperature of 65 °C for varying deposition times of 30, 60, 90, and 120 minutes. Upon completion of each deposition, the coated substrates were first air-dried and then annealed in ambient air at 400 °C for 3 hours.

2.3 ZnO thin films Characterization

The structural properties of the ZnO thin films were examined using an X-ray diffractometer (RIGAKU model) equipped with a CuKα radiation source (λ = 1.54059 Å), with measurements conducted over a 2θ range of 10° to 90° at ambient temperature. Surface morphology was examined via a scanning electron microscope (ZEISS ULTRA 55 model), operated at a low accelerating voltage of 1 kV to minimize charging effects from the glass substrates. The optical properties of the ZnO thin films were evaluated at room temperature using a UV-Vis spectrophotometer (Perkin-Elmer Lambda 800), operating over a wavelength range of 300–900 nm. To identify the functional groups within the films, Fourier-transform infrared (FTIR) spectroscopy was performed using a Perkin-Elmer Spectrum 3 spectrometer, equipped with an attenuated total reflectance (ATR) accessory. Measurements were conducted in transmission mode over the spectral range of 400–4000 cm^{-1} with a resolution of 4 cm^{-1}, and the reported data represent the average of ten scans.

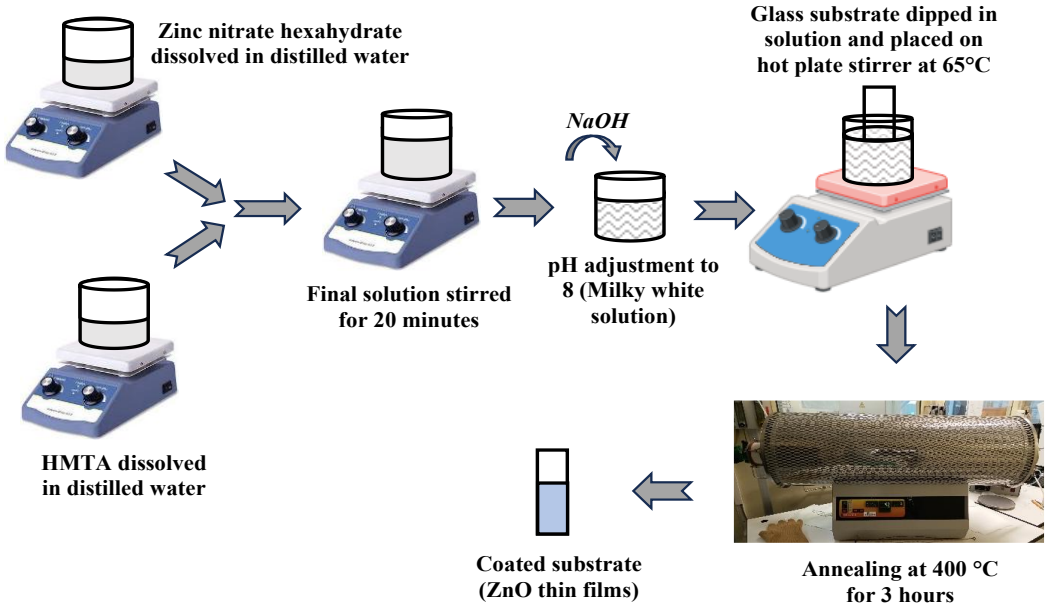

Fig.2 Schematic illustration of the synthesis process of ZnO thin films.

To evaluate the degree of preferred orientation, the texture coefficient ($T_{C(hkl)}$) was determined for the three most intense diffraction peaks using Equation (1) (Romero *et al.*, 2006):

$$T_{C(hkl)} = \frac{\frac{I_{(hkl)}}{I_{0(hkl)}}}{\frac{1}{n}\sum\frac{I_{(hkl)}}{I_{0(hkl)}}} \quad (1)$$

where $I_{(hkl)}$ represents the intensity of the XRD peaks obtained from the synthesized films, $I_{0(hkl)}$ refers to the corresponding standard intensity from the JCPDS card No. 36-1451 for randomly oriented grains, and n is the total number of diffraction peaks considered in the analysis.

The interplanar spacing (d) and lattice parameters (a and c) of the synthesized ZnO thin films were determined using Bragg's law, according to Equations (2) and (3), respectively (Kashif *et al.,* 2012):

$$d = \frac{\lambda}{2\sin\theta} \quad (2)$$

$$a = \sqrt{\frac{1}{3}}\frac{\lambda}{\sin\theta} \text{ and } c = \frac{\lambda}{\sin\theta} \quad (3)$$

Where λ represents CuKα wavelength (1.54059Å) and θ is the diffraction peak angle.

The internal strains along the a-axis (ε_a) and c-axis (ε_c) of ZnO films were determined using Equations (4) and (5), respectively (Ahmed Fattah Abdulrahman *et al.,* 2020).

$$\varepsilon_a = \frac{a - a_0}{a_0} \times 100\% \quad (4)$$

$$\varepsilon_c = \frac{c - c_0}{c_0} \times 100\% \quad (5)$$

Where a_0= 3.249Å and c_0= 5.206Å are the lattice parameters of the standard unconstrained ZnO structure as reported in the JCPDS card 36-1451 (McMurdie *et al.*, 1986).

The crystallite size (D) of the ZnO thin films, corresponding to the dominant (101) diffraction peak, was estimated using the Debye–Scherrer equation (Equation (6)) (Mustapha *et al.,* 2019):

$$D = \frac{k\lambda}{\beta\cos\theta} \quad (6)$$

where k is a constant with a typical value of 0.9, θ represents the Bragg diffraction angle, λ (1.54059 Å) is the wavelength of the X-rays used, and β corresponds to the FWHM of the diffraction peak, expressed in radians.

The dislocation density (δ), which reflects the presence of crystalline imperfections or defects, is estimated using Equation (7) (Mustapha *et al.,* 2019):

$$\delta = \frac{1}{D^2} \quad (7)$$

The unit cell volume (V) of the hexagonal wurtzite structure, along with the Zn–O bond length (L), were calculated using Equations (8) and (9), respectively (Ahmed F. Abdulrahman *et al.*, 2021).

$$V = \left(\frac{\sqrt{3}}{2}\right)a^2c \quad (8)$$

$$L = \sqrt{\frac{a^2}{3} + \left(\frac{1}{2} - u\right)^2 c^2} \quad (9)$$

where (u) represents the internal parameter of the wurtzite structure, reflecting the relative displacement of atoms along the c-axis with respect to the adjacent atomic plane, as defined by Equation (10) (Ahmed F. Abdulrahman *et al.,* 2021):

$$u = \frac{a^2}{3c^2} + 0.25 \quad (10)$$

3. Result and Discussion

3.1 Structural characterization

Fig. 3 presents the XRD patterns of ZnO thin films synthesized on glass substrates at various deposition times. The diffraction peaks observed at planes (100), (002), (101), (102), (110), (103), (200), (112), (201), (004), (202), and (104), with varying intensities, are consistent with the hexagonal wurtzite crystal structure of ZnO, as referenced by the JCPDS card No. 36-1451 (McMurdie *et al.,* 1986). An additional peak is seen around 29° for all the samples, that we attribute to impurities. It is identified to belong to sodium hydroxide monohydrated ($NaOH.H_2O$) using Match software. Based on the NaOH–water phase diagram (Koliverdov, 2010), the formation of this complex in the temperature range of 52°C to 68°C may result from the incomplete dissolution of sodium hydroxide (Hemily, 1957; Wunderlich, 1958).

Table 1 presents the calculated texture coefficients for the (100), (002), and (101) crystallographic planes, derived from the corresponding XRD peak intensities for all samples. These results show that the $T_{C(002)}$ and $T_{C(101)}$ values are slightly less than or approximately equal to 1, indicating a lower growth tendency along these directions compared to the standard JCPDS card 36-1451. In contrast, $T_{C(100)}$ values are slightly greater than 1, suggesting an abundance of grains oriented in this direction, particularly for deposition times between 60 and 90 minutes (Romero *et al.,* 2006). The results confirm that all ZnO thin films are polycrystalline, exhibiting a moderate preferential orientation along the (100) plane, as compared to the standard reference data in JCPDS card No. 36-1451 (Romero *et al.,* 2006). This behavior can be attributed to the anisotropic crystallite growth during the nucleation process (Drici *et al.,* 2004). The distinct and sharp diffraction peaks observed for the ZnO nanoparticles indicate a high degree of crystallinity, consistent with findings reported in the literature (Arellano-Cortaza *et al.,* 2021; Mohan *et al.*, 2024).

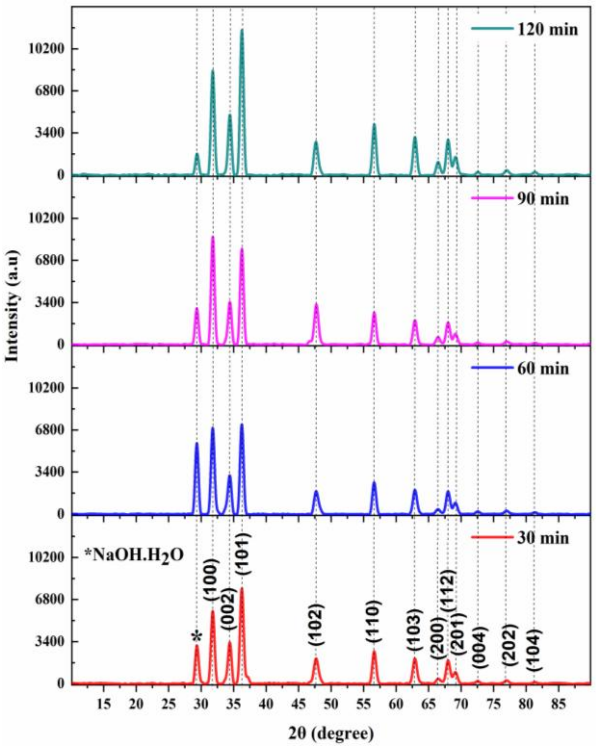

Fig.3 XRD patterns of ZnO mesoporous thin films synthesized at different deposition times.

Table 1
Texture coefficient of ZnO thin films synthesized at different deposition times along the dominant peaks (100), (002) and (101).

Deposition times	$T_{C(hkl)}$		
	(100)	(002)	(101)
30 min	1.2	0.9	0.9
60 min	1.4	0.8	0.8
90 min	1.5	0.8	0.8
120 min	1.2	0.9	1.0

The lattice parameters (a and c) values were reported in Table 2. It can be seen that the obtained a and c values are consistent with the values reported in the JCPDS card No. 36-1451 for ZnO (McMurdie *et al.*, 1986). The interplanar spacing (d) values, calculated using Bragg's law, were consistent across all samples, indicating that the crystal structure of the ZnO thin films remained stable regardless of deposition time. Moreover, the c/a ratio for each sample was approximately 1.60, which aligns well with that of bulk wurtzite ZnO (McMurdie *et al.,* 1986). The consistent c/a ratio indicates several important structural characteristics as : (i) the films maintain their wurtzite phase without significant distortion or phase transitions during fabrication (Morkoç *et al.,* 2008); (ii) a compact lattice arrangement which is beneficial for mechanical and electronic properties of the material (Nizar *et al.,* 2023); (iii) a low density of defects or impurities within the crystal structure suggesting the good crystallinity and fewer disruption in the lattice (Rana *et al.,* 2020).

Table 2 shows the values of the internal strain ε_a and ε_c of ZnO thin films for different deposition times. For all samples, the negative internal strain along the a-axis corresponds to compressive deformation, indicating lattice contraction, while the positive strain along the c-axis reflects tensile deformation, indicating lattice expansion; these strain effects are likely induced by thermal mismatch between the ZnO film and the glass substrate during the annealing process (Mosalagae *et al.,* 2020; Nurizati Rosli *et al.*, 2021). However, the obtained values remain very low, almost negligible, which indicates the good stability of the crystalline structure of the synthesized ZnO thin films (Apeh *et al.*, 2019). Specifically, the internal strain along the a-axis (ε_a) remains stable up to 60 minutes but increases at longer deposition times, indicating higher compressive stress. The internal strain along the c-axis (ε_c) decreases initially, then rises sharply beyond 90 minutes, suggesting vertical stress buildup. These findings reveal that deposition time strongly influences the strain state and structural quality of ZnO thin films, with optimal crystallinity observed between 60 and 90 minutes. Prolonged deposition may lead to stress accumulation and structural distortion due to grain agglomeration (Siregar et al., 2023).

Table 2 shows that the 2θ value for the (101) peak remains nearly constant (~36.27°) across deposition times, with a slight shift toward lower angles at 120 minutes, suggesting minor lattice expansion due to stress relaxation. Meanwhile, the to the full width at half maximum (FWHM) decreases steadily from 0.630° to 0.595°, indicating improved crystallinity and larger crystallite size with longer deposition. This reflects the

Table 2
Lattice parameters and structural characteristics of ZnO mesoporous thin films synthesized at different deposition times alongside (101) peak diffraction.

Deposition times	2θ (°)	FWHM (°)	D (nm)	δ ($\times 10^{15}$ lines/m^2)	Lattice parameters (Å)		c/a ratio	The internal strains along a and c axis		d (Å)	V (Å^3)	L (Å)
					a	c		ε_a (%)	ε_c (%)			
30 min	36.269	0.630	13.269	5.680	3.248	5.210	1.604	-0.031	0.077	2.475	47.599	1.977
60 min	36.271	0.603	13.863	5.203	3.248	5.207	1.603	-0.031	0.019	2.475	47.572	1.977
90 min	36.273	0.600	13.933	5.151	3.247	5.208	1.604	-0.062	0.038	2.475	47.552	1.977
120 min	36.263	0.595	14.049	5.066	3.247	5.213	1.605	-0.062	0.134	2.475	47.597	1.977
JCPDS card 36-1451	36.253	-	-	-	3.250	5.207	1.602	-	-	2.476	47.622	-

progressive coalescence and ordering of ZnO grains during extended CBD growth (Parize *et al.,* 2016).

Table 2 presents the crystallite size and dislocation density values of the ZnO thin films, derived from the dominant (101) diffraction peak for various deposition times. The crystallite size was found to increase from 13.269 nm to 14.049 nm with longer deposition times. This observed variation in crystallite size, especially beyond extended deposition durations, may be attributed to nanoparticle agglomeration that hinders continuous grain growth, as reported by Siregar *et al.* (Siregar *et al.,* 2023). A corresponding decrease in dislocation density was also observed as deposition time increased. These changes can be attributed to variations in crystallite size and internal strain, potentially caused by lattice mismatch between the ZnO films and the glass substrates, as well as nanoparticle aggregation over time. These findings highlight the critical role of deposition time in controlling the properties of ZnO nanostructures synthesized via chemical bath deposition.

Table 2 reveals a slight variation in the unit cell volume (V) of the hexagonal wurtzite structure, while the Zn–O bond length (L) remains nearly constant at 1.977 Å across the different deposition durations. The observed changes in cell volume can be attributed to shifts in the diffraction peak positions (2θ), which directly impact the calculated lattice parameters (a and c). These shifts suggest that the crystal structure of ZnO undergoes subtle modifications as a function of deposition time. The positions of the diffraction peaks (2θ) are highly responsive to alterations in the lattice parameters (a) and (c); therefore, changes in these lattice parameters lead to corresponding modifications in the bond lengths and overall volume of the ZnO crystals formed (Ahmed Fattah Abdulrahman *et al*., 2020). So, the constant in the values of (L) can be explained by the

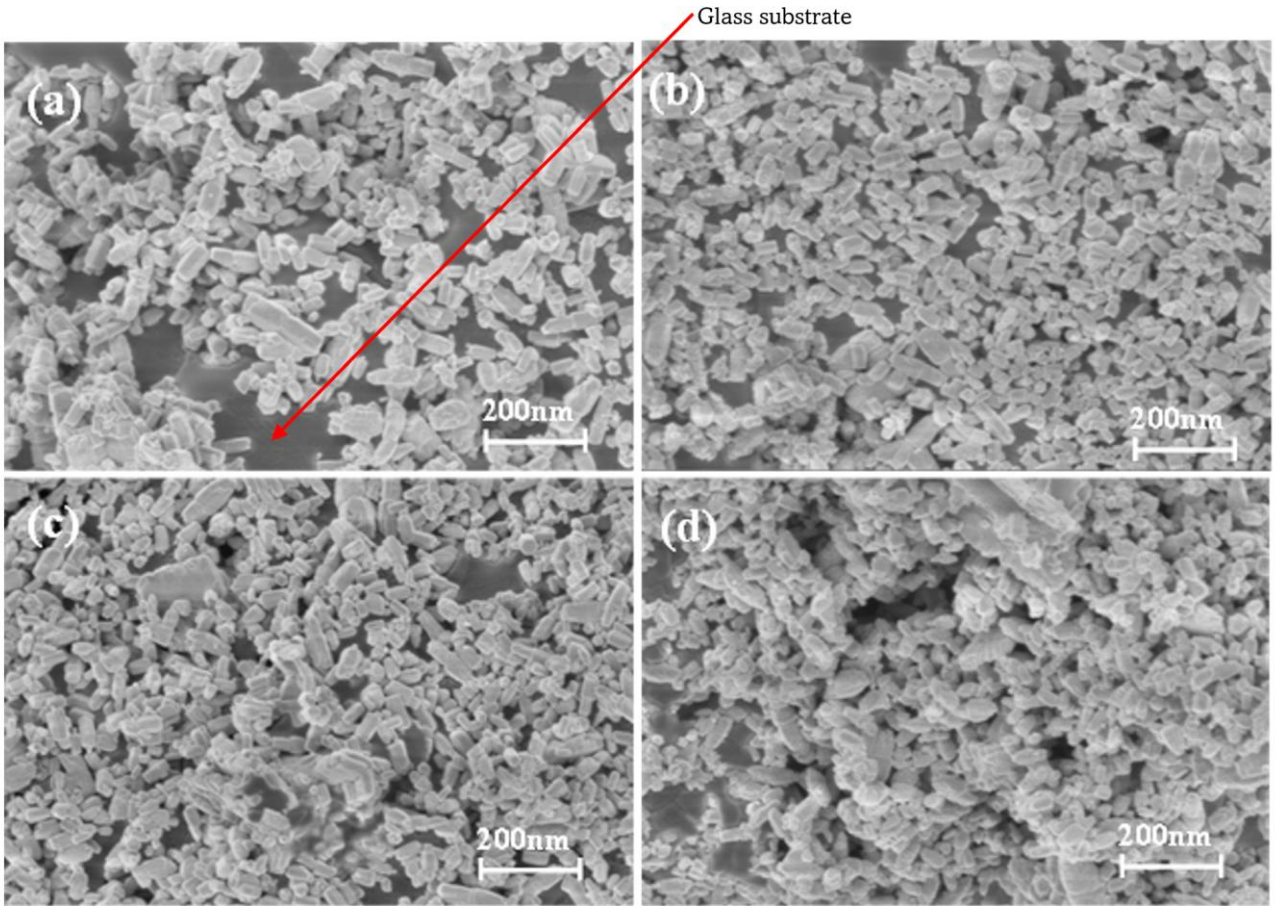

Fig. 4. SEM images of ZnO mesoporous thin films synthesized at (a) 30 min, (b) 60 min, (c) 90 min and (d) 120 min

complementary of the internal strain of the ZnO crystals along the two axes (a and c) (Bindu *et al.,* 2014).

3.2 Morphological Properties

Fig. 4 presents SEM images of ZnO thin films synthetized on glass substrates at varying durations. The images reveal that ZnO microrods are agglomerated and randomly oriented, consistent with the polycrystalline nature of the films suggested by XRD analysis. Furthermore, SEM analysis indicates that the growth of the ZnO microrods on the glass substrates follows Volmer-Weber or 3D growth mode (Oura *et al.,* 2003). At 30 minutes (Fig. 4a), ZnO microrods formed separate islands on the substrate. After 60 minutes (Fig. 4b), the structures arranged themselves in successive layers gradually covering the substrate due to the affinity of precursor with the substrate. For samples obtained at 90 minutes and 120 minutes (Fig. 4c and 4d), growth begins with one or more continuous layers, then forms three-dimensional islands. Moreover, at 120 minutes, it can be seen that microrods are aggregated showing a better recrystallization as confirmed by the XRD results.

Due to the increasing aggregation of ZnO microrods at longer deposition times (90 and 120 minutes), quantitative estimation of film compactness by SEM image analysis was limited. At 30 and 60 minutes, the rods remain well-separated, enabling reliable grain size distributions. However, beyond this point, overlapping structures and secondary growths on microrods hinder accurate measurement. Consequently, a qualitative evaluation of film surface coverage was carried out using ImageJ, which, while approximate, supports the observed trend of increasing film compactness with deposition time. The films become progressively more compact as the deposition time increases. The average microrod diameter, estimated from SEM images, ranges from 65 to 75 nm, with lengths between 155 and 160 nm. Both dimensions show a slight increase with time, reflecting gradual coalescence and densification of the ZnO structures.

3.3 Fourier Transform Infrared (FTIR) analysis

FTIR spectroscopy (4000–400 cm^{-1}) was used to analyze all samples to confirm the formation of ZnO bonds and to identify the presence of organic compounds (Fig. 5). Characteristic Zn–O vibrational modes appeared below 600 cm^{-1}, confirming successful ZnO formation, consistent with our previous works (Ako *et al.,* 2025; Gboglo, Baneto, Gadedjisso-Tossou, *et al.,* 2025).

A peak at 665 cm^{-1} corresponds to =C–H bending vibrations, while the 833 cm^{-1} peak is attributed to H–C–N groups, is assigned by the HMTA material (Idiawati *et al.*, 2017). The stretching vibrations of the C–O bond in primary alcohols is observed at 1240 and 1050 cm^{-1} suggesting the presence of organic residues possibly from incomplete precursor decomposition (Jahan Tamanna *et al.,* 2024). A distinct peak near 1340 cm^{-1} corresponds to H–O–H bending vibrations, indicating the presence of trace amounts of water (H_2O) within the ZnO nanocrystals (Hannachi *et al.,* 2022). This peak occurs for all samples, revealing the hydrophilic behavior of the ZnO thin films. Absorption peaks in the 1780–1650 cm^{-1} range correspond to C=O stretching of amide I and II groups, which may arise from residual organics introduced during synthesis. The absorption band near 2349 cm^{-1} is assigned to carbon dioxide (CO_2) molecules present in the surrounding air (Muthukumaran *et al.,* 2012), whereas the broad peak around 3480 cm^{-1} is linked to the stretching vibrations of hydroxyl (OH) groups, which are probably caused by water molecules adsorbed on the particle surfaces (Arellano-Cortaza *et al.,* 2021).

3.4 Optical properties

Fig. 6 shows the transmittance spectra of ZnO thin films synthesized at different deposition times in the wavelength range from 300 to 900 nm. All samples show transmittance above 50% from visible to infrared, with absorption edges below 350 nm. The highest transmittance, reaching 68%, is observed for ZnO microrods synthesized for 30 minutes, while the lowest value, 52%, corresponds to the sample synthesized for 120 minutes. It is observed that the transmittance value of all ZnO microrods decreases with increasing deposition time, which can be primarily attributed to the increase in film thickness (Idiawati *et al.,* 2017). As deposition time increases, the films become thicker and more compact, leading to enhanced light scattering and absorption. This effect reduces the amount of transmitted light, as confirmed by SEM images showing denser microrod packing. These results are in good

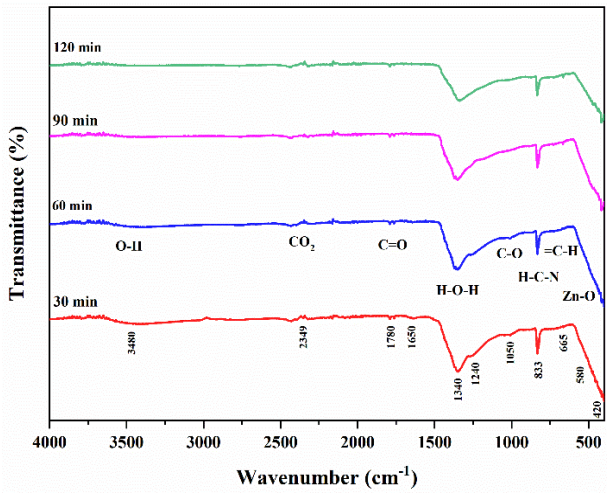

Fig. 5 FTIR spectrum of ZnO mesoporous thin films synthesized at different deposit times.

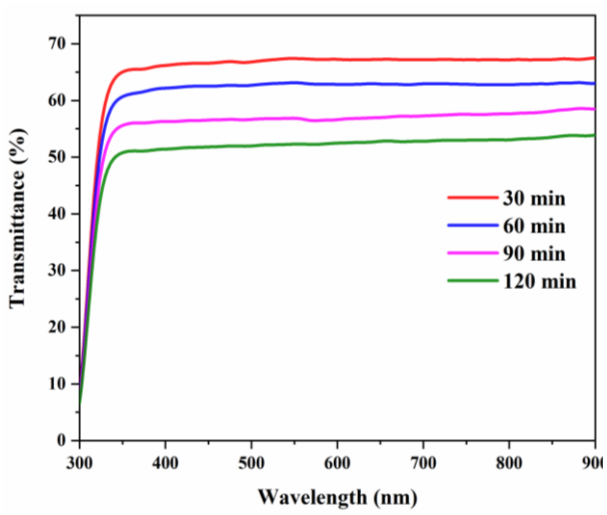

Fig. 6 Optical transmittance spectrum of ZnO mesoporous thin films synthesized at different deposit times.

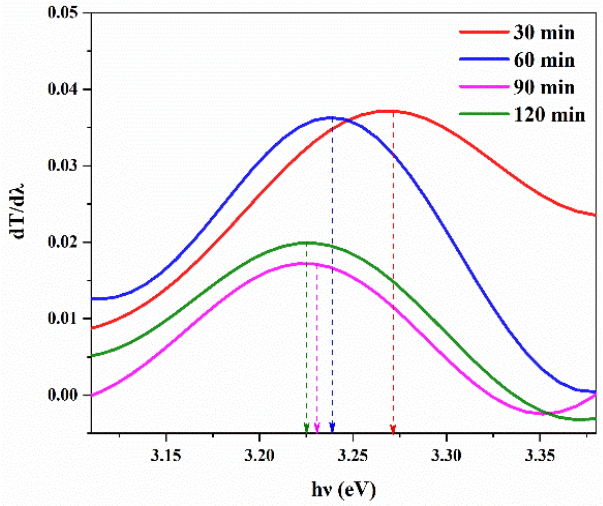

Fig. 7 Optical band gap variations in ZnO mesoporous thin films synthesized at different deposit times.

agreement with those reported in the literature (Idiawati *et al.,* 2017; Rohanieza Abdul Rahman *et al.,* 2020).

To determine the optical band gaps (Eg) of the ZnO samples, the derivative of transmittance with respect to wavelength ($dT/d\lambda$) was calculated. The resulting $dT/d\lambda$ curves were plotted against photon energy ($h\nu$), as shown in Fig. 7, allowing for the extraction of band gap values (Xu *et al.,* 2020). The Eg values obtained for ZnO thin films synthesized at different deposition times are summarized in Table 3. The ZnO thin films exhibit a decrease in band gap energy from 3.27 eV to 3.22 eV with increasing deposition time. This reduction in Eg can be attributed to increased structural disorder within the films. This effect is commonly evaluated through the Urbach energy (Eu), which characterizes the width of the band tail of localized states in the band gap (Urbach, 1953). According to the Urbach model, a plot of $\ln(\alpha)$ versus photon energy ($h\nu$) yields a straight line in the exponential region, whose slope allows the determination of Eu (Malek *et al.,* 2013). Fig. 8 presents the Urbach plots of the films, while the extracted Eu values, obtained from the reciprocal slope of the linear region,

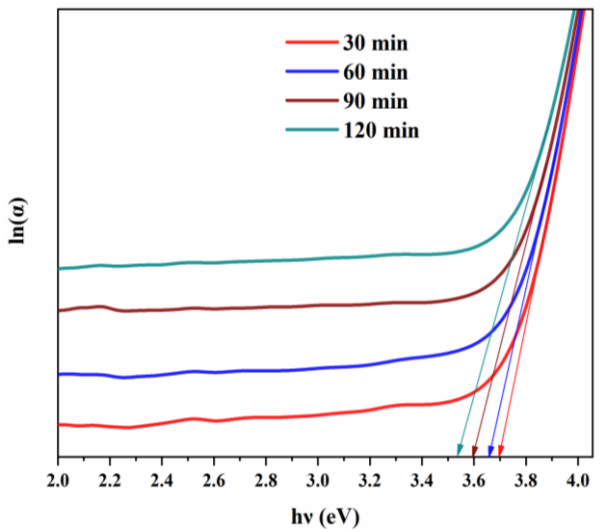

Fig. 8 Curve $\ln(\alpha)$ as a function of $h\upsilon$ for the determination of the Urbach energy of ZnO thin films obtained at different deposition times.

Table 2
Optical band gap and Urbach energy values for ZnO thin films obtained at different deposition times.

Deposition time	Optical band gap (eV)	Urbach energy (meV)
30 min	3.27	270.27
60 min	3.24	273.22
90 min	3.23	277.78
120 min	3.22	282.49

are summarized in Table 3. The results show that Eu increases with deposition time, indicating enhanced structural disorder and a greater density of localized states within the band gap. This trend is consistent with the observed decrease in Eg, as increased disorder promotes band tailing and reduces the effective optical band gap (Anyaegbunam *et al.,* 2018). In general, the band gap values of the synthesized ZnO thin films are slightly lower than that of bulk ZnO (3.37 eV), which may be attributed to internal stress and optical confinement effects associated with ZnO microrod formation (Foo *et al.*, 2014; Marotti, 2004). Furthermore, impurity phases such as $NaOH{\cdot}H_2O$ detected by XRD may also influence the band structure and contribute to these variations.

4. Conclusion

The ZnO thin films synthesized by single-step CBD in this study exhibited high crystallographic quality, as evidenced by XRD patterns confirming a well-defined hexagonal wurtzite structure and good polycrystallinity across all deposition times. This structural stability underlines the reliability of the single-step CBD for synthesizing ZnO films with con-sistent crystal properties. The study highlights that deposition time plays a crucial role in tuning the morphological and optical transmittance of mesoporous ZnO thin films. As deposition time increases, the films become more compact, with denser microrod assemblies and reduced transparency in the visible range. The progressive narrowing of the optical band gap (down to 3.27 eV) may also affect UV absorption characteristics. Reducing deposition time to 30 minutes led to the highest optical transmittance (68%) and the widest band gap (3.22 eV). Overall, these findings confirm that single-step CBD process offers precise and controllable synthesis of ZnO thin films with tailored structural and optical properties.

Acknowledgments

The authors would like to thank the FICCI-DST (Government of India) and the Service de Coopération et d'Action Culturelle (SCAC) of the French Government for their support through the CV Raman International Fellowship Program for African Researchers and the French Government Fellowship Program, respectively.

Author Contributions: Conceptualization, A. D. Gboglo and M. Baneto; methodology, A. D. Gboglo and M. Baneto; formal analysis, O. Ako, K. S. Gadedjisso-Tossou, K. N'Konou and B. Grandidier; data curation, M. Haris, and M. Senthilkumar; writing—original draft, A.D. Gboglo; supervision, M. Baneto, K. N'Konou, M. Haris, and M. Senthilkumar; writing—review and editing, K. S. Gadedjisso-Tossou, K. N'Konou, and B. Grandidier. All authors have read and agreed to the published version of the manuscript.

Funding: This research received financial support from Centre d'Excellence Régional pour la Maîtrise de l'Electricité (CERME) of University of Lomé (crédit IDA 6512-TG, Don IDA 536IDA).

Conflicts of Interest: The authors declare no conflict of interest.

References

Abdulrahman, Ahmed F., Ahmed, S. M., Hamad, S. M., Almessiere, M. A., Ahmed, N. M., & Sajadi, S. M. (2021). Effect of different pH values on growth solutions for the ZnO nanostructures. *Chinese Journal of Physics*, *71*, 175–189. https://doi.org/10.1016/j.cjph.2021.02.013

Abdulrahman, Ahmed Fattah, Ahmed, S. M., Ahmed, N. M., & Almessiere, M. A. (2020). Enhancement of ZnO Nanorods Properties Using Modified Chemical Bath Deposition Method: Effect of Precursor Concentration. *Crystals*, *10*(5), 386. https://doi.org/10.3390/cryst10050386

Ako, O., Baneto, M., Senthilkumar, M., Haris, M., Gboglo, A. D., Gadedjisso-Tossou, K. S., Ahyi, A. C., Beltako, K., & Amou, K. A. (2025). Simultaneous effect of precursor sources and precursor concentration on structural, morphological and optical properties of ZnO nanostructured thin films for photovoltaic applications. *International Journal of Renewable Energy Development*, *0*(0). https://doi.org/10.61435/ijred.2025.61069

Aksoy, S., Polat, O., Gorgun, K., Caglar, Y., & Caglar, M. (2020). Li doped ZnO based DSSC: Characterization and preparation of nanopowders and electrical performance of its DSSC. *Physica E: Low-Dimensional Systems and Nanostructures*, *121*, 114127. https://doi.org/10.1016/j.physe.2020.114127

Anyaegbunam, F. N. C., & Augustine, C. (2018). A study of optical band gap and associated urbach energy tail of chemically deposited metal oxides binary thin films. *Digest Journal of Nanomaterials and Biostructures*, *13*(3), 847–856.

Apeh, O. O., Chime, U. K., Agbo, S., Ezugwu, S., Taziwa, R., Meyer, E., Sutta, P., Maaza, M., & Ezema, F. I. (2019). Properties of nanostructured ZnO thin films synthesized using a modified aqueous chemical growth method. *Materials Research Express*, *6*(5), 056406. https://doi.org/10.1088/2053-1591/aadcd6

Arellano-Cortaza, M., Ramírez-Morales, E., Pal, U., Pérez-Hernández, G., & Rojas-Blanco, L. (2021). pH dependent morphology and texture evolution of ZnO nanoparticles fabricated by microwave-assisted chemical synthesis and their photocatalytic dye degradation activities. *Ceramics International*, *47*(19), 27469–27478. https://doi.org/10.1016/j.ceramint.2021.06.170

Bindu, P., & Thomas, S. (2014). Estimation of lattice strain in ZnO nanoparticles: X-ray peak profile analysis. *Journal of Theoretical and Applied Physics*, *8*(4), 123–134. https://doi.org/10.1007/s40094-014-0141-9

Drici, A., Djeteli, G., Tchangbedji, G., Derouiche, H., Jondo, K., Napo, K., Bernède, J. C., Ouro-Djobo, S., & Gbagba, M. (2004). Structured ZnO thin films grown by chemical bath deposition for photovoltaic applications. *Physica Status Solidi (a)*, *201*(7), 1528–1536. https://doi.org/10.1002/pssa.200306806

Elen, K., Van Den Rul, H., Hardy, A., Van Bael, M. K., D'Haen, J., Peeters, R., Franco, D., & Mullens, J. (2009). Hydrothermal synthesis of ZnO nanorods: a statistical determination of the significant parameters in view of reducing the diameter. *Nanotechnology*, *20*(5), 055608. https://doi.org/10.1088/0957-4484/20/5/055608

Fekadu, G. H., & Tizazu, A. (2019). Short Review of Factors Affecting Chemical Bath Deposition Method for Metal Chalcogenide Thin Films. *International Journal of Thin Film Science and Technology*, *8*(2), 43–53. http://dx.doi.org/10.18576/ijtfst/080203

Foo, K. L., Hashim, U., Muhammad, K., & Voon, C. H. (2014). Sol–gel synthesized zinc oxide nanorods and their structural and optical investigation for optoelectronic application. *Nanoscale Research Letters*, *9*(1). https://doi.org/10.1186/1556-276x-9-429

Gan, Y. K., Zakaria, N. F., Mohamad, I. S., & Norizan, M. N. (2020). *The effect of ZnO photoanode solution ageing to the performance of dye-sensitized solar cell (DSSC)*. 020048. https://doi.org/10.1063/1.5142140

Gboglo, A. D., Baneto, M., Ako, O., Haris, M., & Senthilkuma, M. (2025). Role of hexamethylenetetramine/zinc nitrate hexahydrate molar ratio in controlling structural, morphological and optical properties of ZnO thin films synthesized by CBD. *AIMS Materials Science*, *12*(4), 893–908. https://doi.org/10.3934/matersci.2025039

Gboglo, A. D., Baneto, M., Gadedjisso-Tossou, K. S., Ako, O., Ahyi, A. C., Haris, M., Senthilkumar, M., N'konou, K., Grandidier, B., Beltako, K., Amou, K. A., & Dzagli, M. M. (2025). Co-Effect of pH Control Agent and pH Value on the Physical Properties of ZnO Thin Films Obtained by Chemical Bath Deposition for Potential Application in Dye-Sensitized Solar Cells. *Surfaces*, *8*(3), 46. https://doi.org/10.3390/surfaces8030046

George, A., Kumari, P., Soin, N., Roy, S. S., & McLaughlin, J. A. (2010). Microstructure and field emission characteristics of ZnO nanoneedles grown by physical vapor deposition. *Materials Chemistry and Physics*, *123*(2–3), 634–638. https://doi.org/10.1016/j.matchemphys.2010.05.029

Hamelmann, F. U. (2014). Transparent Conductive Oxides in Thin Film Photovoltaics. *Journal of Physics: Conference Series*, *559*, 012016. https://doi.org/10.1088/1742-6596/559/1/012016

Hannachi, E., Slimani, Y., Nawaz, M., Trabelsi, Z., Yasin, G., Bilal, M., Almessiere, M. A., Baykal, A., Thakur, A., & Thakur, P. (2022). Synthesis, characterization, and evaluation of the photocatalytic properties of zinc oxide co-doped with lanthanides elements. *Journal of Physics and Chemistry of Solids*, *170*, 110910. https://doi.org/10.1016/j.jpcs.2022.110910

Hassan, N. K., Hashim, M. R., & Al-Douri, Y. (2014). Morphology and optical investigations of ZnO pyramids and nanoflakes for optoelectronic applications. *Optik*, *125*(11), 2560–2564. https://doi.org/10.1016/j.ijleo.2013.10.023

He, Y., Hu, J., & Xie, Y. (2015). High-efficiency dye-sensitized solar cells of up to 8.03% by air plasma treatment of ZnO nanostructures. *Chemical Communications*, *51*(90), 16229–16232. https://doi.org/10.1039/C5CC04567C

Hemily, P. W. (1957). Structures cristallines des hydrates de la soude. I. Structure cristalline de NaOH.4H $_2$ O. *Acta Crystallographica*, *10*(1), 37–44. https://doi.org/10.1107/S0365110X57000092

Hosono, H., & Ueda, K. (2017). Transparent Conductive Oxides. In S. Kasap & P. Capper (Eds.), Springer Handbook of Electronic and Photonic Materials (pp. 1391–1404). Cham: Springer International Publishing. https://doi.org/10.1007/978-3-319-48933-9_58

Idiawati, R., Mufti, N., Taufiq, A., Wisodo, H., Laila, I. K. R., Fuad, A., & Sunaryono. (2017). Effect of Growth Time on the Characteristics of ZnO Nanorods. *IOP Conference Series: Materials Science and Engineering*, *202*, 012050. https://doi.org/10.1088/1757-899X/202/1/012050

Jahan Tamanna, N., Sahadat Hossain, Md., Mohammed Bahadur, N., & Ahmed, S. (2024). Green synthesis of Ag2O & facile synthesis of ZnO and characterization using FTIR, bandgap energy & XRD (Scherrer equation, Williamson-Hall, size-train plot, Monshi-Scherrer model). *Results in Chemistry*, *7*, 101313. https://doi.org/10.1016/j.rechem.2024.101313

Kashif, M., Hashim, U., Ali, M. E., Ali, S. M. U., Rusop, M., Ibupoto, Z. H., & Willander, M. (2012). Effect of Different Seed Solutions on the Morphology and Electrooptical Properties of ZnO Nanorods. *Journal of Nanomaterials*, *2012*, 1–6. https://doi.org/10.1155/2012/452407

Khorsand Zak, A., Majid, W. H. abd., Wang, H. Z., Yousefi, R., Moradi Golsheikh, A., & Ren, Z. F. (2013). Sonochemical synthesis of hierarchical ZnO nanostructures. *Ultrasonics Sonochemistry*, *20*(1), 395–400. https://doi.org/10.1016/j.ultsonch.2012.07.001

Kim, S. A., Abbas, M. A., Lee, L., Kang, B., Kim, H., & Bang, J. H. (2016). Control of morphology and defect density in zinc oxide for improved dye-sensitized solar cells. *Physical Chemistry Chemical Physics*, *18*(44), 30475–30483. https://doi.org/10.1039/C6CP04204J

Koliverdov, V. F. (2010). Relation between the temperature coefficient of surface tension and phase diagrams. *Russian Journal of Physical Chemistry A*, *84*(8), 1294–1300. https://doi.org/10.1134/S0036024410080042

Kuo, S.-Y., Yang, J.-F., & Lai, F.-I. (2014). Improved dye-sensitized solar cell with a ZnO nanotree photoanode by hydrothermal method.

Nanoscale Research Letters, *9*(1), 206. https://doi.org/10.1186/1556-276X-9-206

Liu, H., Avrutin, V., Izyumskaya, N., Özgür, Ü., & Morkoç, H. (2010). Transparent conducting oxides for electrode applications in light emitting and absorbing devices. *Superlattices and Microstructures*, *48*(5), 458–484. https://doi.org/10.1016/j.spmi.2010.08.011

Liyana, G. R., Sofyan, N., Dhaneswara, D., Subhan, A., & Yuwono, A. H. (2020). *Optoelectronic properties of ZnO nanorods thin films derived from chemical bath deposition with different growth times*. 030008. https://doi.org/10.1063/5.0015869

Look, D. C., Reynolds, D. C., Sizelove, J. R., Jones, R. L., Litton, C. W., Cantwell, G., & Harsch, W. C. (1998). Electrical properties of bulk ZnO. *Solid State Communications*, *105*(6), 399–401. https://doi.org/10.1016/S0038-1098(97)10145-4

Lupan, O., Guérin, V. M., Ghimpu, L., Tiginyanu, I. M., & Pauporté, T. (2012). Nanofibrous-like ZnO layers deposited by magnetron sputtering and their integration in dye-sensitized solar cells. *Chemical Physics Letters*, *550*, 125–129. https://doi.org/10.1016/j.cplett.2012.08.071

Magiswaran, K., Norizan, M. N., Mahmed, N., Mohamad, I. S., Idris, S. N., Sabri, M. F. M., Amin, N., Sandu, A. V., Vizureanu, P., Nabiałek, M., & Salleh, M. A. A. M. (2022). Controlling the Layer Thickness of Zinc Oxide Photoanode and the Dye-Soaking Time for an Optimal-Efficiency Dye-Sensitized Solar Cell. *Coatings*, *13*(1), 20. https://doi.org/10.3390/coatings13010020

Malek, M. F., Mamat, M. H., Sahdan, M. Z., Zahidi, M. M., Khusaimi, Z., & Mahmood, M. R. (2013). Influence of various sol concentrations on stress/strain and properties of ZnO thin films synthesised by sol–gel technique. *Thin Solid Films*, *527*, 102–109. https://doi.org/10.1016/j.tsf.2012.11.095

Marotti, R. (2004). Bandgap energy tuning of electrochemically grown ZnO thin films by thickness and electrodeposition potential. *Solar Energy Materials and Solar Cells*, *82*(1–2), 85–103. doi: 10.1016/j.solmat.2004.01.008

McMurdie, H. F., Morris, M. C., Evans, E. H., Paretzkin, B., Wong-Ng, W., Ettlinger, L., & Hubbard, C. R. (1986). Standard X-Ray Diffraction Powder Patterns from the JCPDS Research Associateship. *Powder Diffraction*, *1*(2), 64–77. https://doi.org/10.1017/S0885715600011593

Mohan, V. K., Srivastav, A., Güell, F., & John, T. T. (2024). pH-controlled synthesis of ZnO nanoflowers: A correlation study among the optoelectronic properties and improved photodegradation efficiency. *Journal of Alloys and Compounds*, *976*, 172993. https://doi.org/10.1016/j.jallcom.2023.172993

Morkoç, H., & Özgür, Ü. (2008). *Zinc Oxide: Fundamentals, Materials and Device Technology*. John Wiley & Sons.

Mosalagae, K., Murape, D. M., & Lepodise, L. M. (2020). Effects of growth conditions on properties of CBD synthesized ZnO nanorods grown on ultrasonic spray pyrolysis deposited ZnO seed layers. *Heliyon*, *6*(7), e04458. https://doi.org/10.1016/j.heliyon.2020.e04458

Mustapha, S., Ndamitso, M. M., Abdulkareem, A. S., Tijani, J. O., Shuaib, D. T., Mohammed, A. K., & Sumaila, A. (2019). Comparative study of crystallite size using Williamson-Hall and Debye-Scherrer plots for ZnO nanoparticles. *Advances in Natural Sciences: Nanoscience and Nanotechnology*, *10*(4), 045013. https://doi/org/10.1088/2043-6254/ab52f7

Muthukumaran, S., & Gopalakrishnan, R. (2012). Structural, FTIR and photoluminescence studies of Cu doped ZnO nanopowders by co-precipitation method. *Optical Materials*, *34*(11), 1946–1953. https://doi.org/10.1016/j.optmat.2012.06.004

Nizar, B. M., Lajnef, M., Chaste, J., Chtourou, R., & Herth, E. (2023). Highly C-oriented (002) plane ZnO nanowires synthesis. *RSC Advances*, *13*(22), 15077–15085. https://doi.org/10.1039/D3RA01511D

Ohodnicki, P. R., Wang, C., & Andio, M. (2013). Plasmonic transparent conducting metal oxide nanoparticles and nanoparticle films for optical sensing applications. *Thin Solid Films*, *539*, 327–336. https://doi.org/10.1016/j.tsf.2013.04.145

Oura, K., Katayama, M., Zotov, A. V., Lifshits, V. G., & Saranin, A. A. (2003). *Surface Science*. Berlin, Heidelberg: Springer Berlin Heidelberg. https://doi.org/10.1007/978-3-662-05179-5

Parihar, V., Raja, M., & Paulose, R. (2018). A Brief Review of Structural, Electrical and Electrochemical Properties of Zinc Oxide Nanoparticles. *Reviews on Advanced Materials Science*, *53*(2), 119–130. https://doi.org/10.1515/rams-2018-0009

Parize, R., Garnier, J., Chaix-Pluchery, O., Verrier, C., Appert, E., & Consonni, V. (2016). Effects of Hexamethylenetetramine on the Nucleation and Radial Growth of ZnO Nanowires by Chemical Bath Deposition. *The Journal of Physical Chemistry C*, *120*(9), 5242–5250. https://doi.org/10.1021/acs.jpcc.6b00479

Rahman, R. A., Zulkefle, M. A., Herman, S. H., & Alip, R. I. (2019). Synthesis of Zinc Oxide Nanostructure by Chemical Bath Deposition (CBD) Method: Influence of Growth Time towards Nanostructure Characteristics. *International Journal of Recent Technology and Engineering (IJRTE)*, *8*(4), 6891–6896. https://doi.org/10.35940/ijrte.D5212.118419

Rahman, Rohanieza Abdul, Zulkefle, M. A., Herman, S. H., & Alip, R. I. (2020). *Study on ZnO nanostructures characteristics: Growth time dependence*. 020010. doi: 10.1063/5.0032850

Rana, A. U. H. S., Shaikh, S. F., Al-Enizi, A. M., Agyeman, D. A., Ghani, F., Nah, I. W., & Shahid, A. (2020). Intrinsic Control in Defects Density for Improved ZnO Nanorod-Based UV Sensor Performance. *Nanomaterials*, *10*(1), 142. https://doi.org/10.3390/nano10010142

Romero, R., Leinen, D., Dalchiele, E. A., Ramos-Barrado, J. R., & Martín, F. (2006). The effects of zinc acetate and zinc chloride precursors on the preferred crystalline orientation of ZnO and Al-doped ZnO thin films obtained by spray pyrolysis. *Thin Solid Films*, *515*(4), 1942–1949. https://doi.org/10.1016/j.tsf.2006.07.152

Rosli, N, Halim, M. M., Hashim, M. R., Maryam, W., Rusdi, M. F. M., & Muhammad, A. R. (2020). Effect of the Seeding Thickness on the Growth of ZnO Nanorods prepared by CBD. *IOP Conference Series: Materials Science and Engineering*, *854*(1), 012074. https://doi.org/10.1088/1757-899X/854/1/012074

Rosli, Nurizati, Halim, M. M., & Hashim, M. R. (2021). Effect of CBD growth times on the ZnO microrods prepared on macroporous silicon. *Applied Physics A*, *127*(9), 712. https://doi.org/10.1007/s00339-021-04865-3

Schaper, N., Alameri, D., Kim, Y., Thomas, B., McCormack, K., Chan, M., Divan, R., Gosztola, D. J., Liu, Y., & Kuljanishvili, I. (2021). Controlled Fabrication of Quality ZnO NWs/CNTs and ZnO NWs/Gr Heterostructures via Direct Two-Step CVD Method. *Nanomaterials*, *11*(7), 1836. https://doi.org/10.3390/nano11071836

Siregar, N., Motlan, M., Sirait, M. (2023). Electroplated ZnO Thin Film: Influence of Deposition Time on Optical and Structural Properties. *Journal of Physical Science*, *34*(1), 43–55. https://doi.org/10.21315/jps2023.34.1.4

Tirtha, R. A., Dinesh Kumar, C., Sandhya, G., Amrendra, K. S., Rajesh, S., Pradeep, L., Bishwa, C. A., Prajwal, L., Bhupal, P., Nagendra, K. K., & Eun, H. C. (2022). Effects of Deposition Time on The Formaldehyde Sensing Ability of Zno Thin Films at Room Temperature. *SSRN Electronic Journal*. https://doi.org/10.2139/ssrn.4264066

Ungula J, Kiprotich S, & Swart HC. (2024). Effect of Deposition Time on Material Properties of ZnO Nanorods Grown on GZO Seed Layer by CBD. *Journal of Nanosciences Research & Reports*, *6*(1), 1–6. https://doi.org/10.47363/JNSRR/2024(6)156

Urbach, F. (1953). The Long-Wavelength Edge of Photographic Sensitivity and of the Electronic Absorption of Solids. *Physical Review*, *92*(5), 1324–1324. https://doi.org/10.1103/PhysRev.92.1324

Wang, S.-F., Tseng, T.-Y., Wang, Y.-R., Wang, C.-Y., & Lu, H.-C. (2009). Effect of ZnO seed layers on the solution chemical growth of ZnO nanorod arrays. *Ceramics International*, *35*(3), 1255–1260. https://doi.org/10.1016/j.ceramint.2008.06.012

Wen, H., Weng, B., Wang, B., Xiao, W., Liu, X., Wang, Y., Zhang, M., & Huang, H. (2024). Advancements in Transparent Conductive Oxides for Photoelectrochemical Applications. *Nanomaterials*, *14*(7), 591. https://doi.org/10.3390/nano14070591

Wu, M.-S., & Yang, R.-S. (2018). Post-treatment of porous titanium dioxide film with plasmonic compact layer as a photoanode for enhanced dye-sensitized solar cells. *Journal of Alloys and Compounds*, *740*, 695–702. https://doi.org/10.1016/j.jallcom.2018.01.032

Wunderlich, J. A. (1958). Contribution à l'étude cristallochimique des hydrates de soude. I. — Méthodes expérimentales et les

structures cristallines de NaOH.H2O et de 2 NaOH.7 H2O. *Bulletin de la Société française de Minéralogie et de Cristallographie*, *81*(10), 287–314. https://doi.org/10.3406/bulmi.1958.5288

Xiao-bo, L., Hong-lie, S., Hui, Z., & Bin-bin, L. (2007). Optical properties of nanosized ZnO films prepared by sol-gel process. *Trans. Nonferrous Met. Soc. China*.

Xu, L., Wang, X., Qian, L., Zhu, Y., Luo, X., Wang, W., Xu, X., & Xu, J. (2020). The dependence of the optical properties of ZnO nanorod arrays on their growth time. *Optik*, *202*, 163634. https://doi:.org/10.1016/j.ijleo.2019.163634

Xu, S., Fang, D., Xiong, F., Ren, Y., Bai, C., Mi, B., & Gao, Z. (2023). Electrophoretic deposition of double-layer ZnO porous films for DSSC photoanode. *Journal of Solid State Electrochemistry*. https://doi.org/10.1007/s10008-023-05708-2

.